Computation of the noise generated by low Mach number flows around a cylinder and a wall-mounted half-cylinder

F. Pérot* , J.M. Auger† and H. Giardi‡
PSA Peugeot Citroën
Centre Technique de Vélizy
4 route de Gisy, 78943 Vélizy Villacoublay, France

C. Bailly § and D. Juvé ¶
Laboratoire de Mécanique des Fluides et d'Acoustique
Ecole Centrale de Lyon & UMR CNRS 5509
36 avenue Guy de Collongue, 69134 Ecully, France

For modern cars, aerodynamic noise is becoming the major source of annoyance during peri-urban trips. To take this point into consideration from the vehicle development and to improve the interior comfort, appropriate numerical methods have to be developed. The estimation of the broadband noise generated by low Mach number flows about M$\sim$0.1, considered in this study, are obtained by applying a two-step method combining incompressible CFD calculations with acoustic analogy.
In this paper, the advanced-time algorithm is developed to allow the estimation of all the terms of Ffowcs Williams and Hawkings' equation and particularly the volume terms. The noise corresponding to a cylinder flow is then used to validate this approach and to compute the broadband noise radiated by a 3-D incompressible and turbulent flow.
The algorithm is then applied to a wall-mounted half-cylinder corresponding to a simplified side-mirror shape. In order to validate the half-cylinder aeroacoustic calculations, the numerical results are favourably compared to measurements recently carried out.

I. Introduction

For automotive, the acoustic interior comfort has an increasing importance and becomes a selection criterion for consumers. The major source of annoyance above 400 Hz and for speeds in excess of 100 km/h is the aerodynamic noise, generated both by the shape of the car and by exterior accessories such as the side-mirrors. However the aerodynamic noise production is a complex phenomenom and its reduction remains an experimental art. The improvement and the time-reduction of the car design is then closely connected to the developement of numerical tools able to estimate the aeroacoustic sound.

*PhD student, franck.perot@mpsa.com, AIAA member
†Research engineer, jeanmarc.auger@mpsa.com
‡Research engineer, helene.giardi@mpsa.com
§Professor, christophe.bailly@ec-lyon.fr, AIAA member
¶Professor, daniel.juve@ec-lyon.fr, AIAA member

Up to now, aeroacoustic computations remain in the research domain for automotive applications. On the one hand, hybrid methods and simplified source models based on statistical properties of the turbulence, provide only rough estimation of the radiation sound and a poor understanding of the physical mechanisms involved in the noise production. On the other hand, source modeling based on unsteady aerodynamic results are very time consuming but will become more relevant as long as computation power is growing.
The present paper investigates such an approach based on the spatio-temporal resolution of Ffowcs Williams and Hawkings' (FW-H) equation. Starting from unsteady incompressible CFD results, an advanced time algorithm is used to derive an estimation of the far-field radiated noise involving both the contribution of surface and volume integrals. By applying this method, results regarding the influence of each integral contribution on both the tonal noise and broadband noise are discussed by analyzing two test cases :

- the 3-D cylinder as an extension of the previous work performed by the authors.[1]
- the wall mounted half cylinder as a simplified automotive case for which an experimental and a numerical analysis are presented.

II. Aeroacoustic computational method

The estimation of the acoustic pressure p'_a radiated by an incompressible and low Mach number flow in presence of a steady and rigid wall is performed by solving FW-H's equation in the time domain[2,3] :

$$\begin{aligned} 4\pi p'_a(\mathbf{x},t) &= \frac{1}{c_\infty^2}\frac{\partial^2}{\partial t^2}\iiint_V \left[\frac{r_i r_j}{r^3}T_{ij}\right]_{\tau^*} d\mathbf{y} + \frac{1}{c_\infty}\frac{\partial}{\partial t}\iiint_V \left[\left(3\frac{r_i r_j}{r^4} - \frac{\delta_{ij}}{r^2}\right)T_{ij}\right]_{\tau^*} d\mathbf{y} \\ &+ \iiint_V \left[\left(3\frac{r_i r_j}{r^5} - \frac{\delta_{ij}}{r^3}\right)T_{ij}\right]_{\tau^*} d\mathbf{y} + \frac{1}{c_\infty}\frac{\partial}{\partial t}\iint_\Sigma \left[\frac{r_i}{r^2}P_{ij}n_j\right]_{\tau^*} d\Sigma + \iint_\Sigma \left[\frac{r_i}{r^3}P_{ij}n_j\right]_{\tau^*} d\Sigma \quad (1) \end{aligned}$$

where, $T_{ij} = \rho_\infty u_i u_j$ is Lighthill's tensor, $P_{ij} = p\delta_{ij}$, u_i are the velocity components and p the hydrodynamic pressure in our case. The geometric coordinates are defined as $r_i = x_i - y_i$ and $r = |\mathbf{x} - \mathbf{y}|$. The unit vector $\mathbf{n}$ is the normal to the surface Σ and V corresponds to the integration volume where the flow is solved. The notation τ^* means that the source terms are estimated at the retarded times $\tau^* = t - r/c_\infty$ to take into account the propagation of the sound waves from $\mathbf{y}$ to $\mathbf{x}$.

To compute the acoustic far-field pressure verifying $\mathbf{x} \gg \mathbf{y}$, only the first and the forth right hand terms of equation (1) are retained. As a result, the following expression gives an estimate of the far-field noise :

$$4\pi p'_a(\mathbf{x},t) = \frac{1}{c_\infty^2}\frac{\partial^2}{\partial t^2}\iiint_V \left[\frac{r_i r_j}{r^3}T_{ij}\right]_{\tau^*} d\mathbf{y} + \frac{1}{c_\infty}\frac{\partial}{\partial t}\iint_\Sigma \left[\frac{r_i}{r^2}P_{ij}n_j\right]_{\tau^*} d\Sigma \quad (2)$$

Note that equation (2) is equivalent to Curle's formulation.

To solve equations (1) and (2), an advanced-time method (also called source-time dominant algorithm) is developed according to the approach used for many years to compute for instance helicopter noise.[4] The principle of this approach is to evaluate the radiated sound on $\mathbf{x}$ at the time $t = \tau^* + r/c_\infty$, τ^* being now chosen as the time when the source terms are known, *i.e.* the time steps of the aerodynamic simulation. Such a method avoids the storage of the source terms and simplifies the manipulation of the databases : the calculation of all the terms is then reachable for 3-D applications and particularly the volume integrals.

The derivation of the source terms is performed using classical centred differentiating schemes. The first and second derivatives of a function ψ at time i are computed with the following schemes :

$$\left(\frac{\partial\psi}{\partial t}\right)_i = \frac{\psi_{i+1} - \psi_{i-1}}{2\Delta t} \quad \text{and,} \quad \left(\frac{\partial^2\psi}{\partial t^2}\right)_i = \frac{(\psi_{i+1} - 2\psi_i + \psi_{i-1})}{\Delta t^2} \quad (3)$$

Higher order schemes have been tested but they do not provide more accurate results. One of the problems generated by the time derivation is the introduction of high frequency noise. To limit such a phenomenon a temporal filtering based on selective filters developed by Bogey and Bailly[5] is implemented in the aeroacoustic calculations.
The interpolation of the acoustic pressure signals is performed using Lagrange polynomials of the third degree. The surface and volume integrations are computed using a Gaussian quadrature method of the third and second order.

The last point to be processed is the numerical noise generated by the vortices crossing the outlet boundary of the aerodynamic domain.[6] For direct noise computations, a sponge zone absorbing the aerodynamic quantities and the acoustic waves is used.[7,8] However, for an incompressible computation such a treatment is not used. In order to decrease the noise by the truncature, the source volume is spatially windowed using the following function :

$$f(x_1) = 1 - \exp\left(\frac{(x_1 - x_{1max})^2}{2\sigma^2}\right) \tag{4}$$

The determination of σ depends on the data which have to be windowed. A robust method is used to determine σ as the value verifying for instance $f(x_f) = 0.7$, x_f being a characteristic length preliminary chosen. The different tests performed have shown that the windowing had to be applied to a large zone. For example, on the following test case of the 3-D cylinder, the characteristic length of the vortices is D, and the value $x_f = 12.5D$ has been used.

III. The cylinder noise

For cylinder flows, the noise generated by the æolian tone is well estimated by only taking into account the surface integral. Physically, this term corresponds to the diffraction of the flow sources by the rigid body which is much more efficient than the direct radiation field involved in the volume integral for compact sources and low frequency noise.[1,9,10]

However, as our aim is also to study the broadband noise, the evaluation of all the terms of the FW-H's equation seems required. In this part, the advanced time method is used on a 3-D LES simulation around a cylinder and a comparison of the two terms of equation (2) up to $3-4$ kHz is proposed .

A. Aerodynamic simulation

The aerodynamic simulation used here is the same as the one presented in Pérot *et al.*, that is a 3-D incompressible LES simulation performed over a circular cylinder at $\mathrm{Re}_D = 1.4 \times 10^5$ and $\mathrm{M} = 0.16$. The diameter of the cylinder is $D = 3.81$ cm and the spanwise dimension is $L_Z = 1.5D$. The computational domain extends from $-4D$ to $18D$ in the x_1-direction, and from $-5D$ to $5D$ in the x_2-direction.
To reduce both the computational time and the size of the total mesh-grid, and to increase the time step, a wall-layer model has been introduced.[11,12] This model smoothes the problem related to transition mechanisms in the boundary layer and its major restriction is a poor prediction of the position of the boundary layer detachments ($\theta_s = 110^o$ instead of $\theta_s = 80^o$). The LES of the FLUENT code has been used. The Smagorinsky subgrid-scale model is retained with a constant adjusted to $C_s = 0.12$. The time step of the simulation is $\Delta t = 10^{-5}$ s, and about 0.1 s of physical time is stored.

The frequency of the vortex shedding is $f_0 = 403$ Hz and the corresponding Strouhal number is St$= Df_0/U_\infty = 0.27$. The coherent structures in the wake are plotted in figure 1. This value corresponds to a transcritical flow for which the boundary layers are turbulent from the stagnation point to the detachments induced by the wall model. The value of the drag coefficient is $\bar{C}_D = 0.71$ and favourably compares to Batham's measurements[13] obtained with a rough cylinder corresponding to an artificial turbulent state.
The predicted flow in term of mean and fluctuating values is also in good agreement with the measurements

of Cantwell & Coles[14] and other simulations of the literature[15–17] (figure 2 for instance), and the evaluation of its acoustic radiation should give satisfying results.

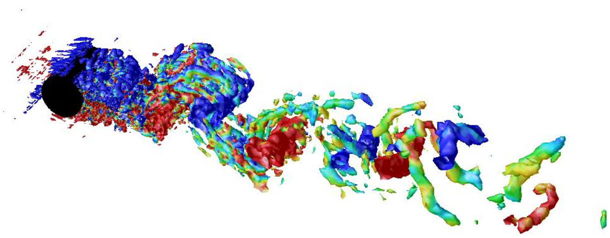

Figure 1. Perspective view of the Q-criterion ($Q = -\frac{1}{2}u_{i,j}u_{j,i}$) for a circular cylinder, isosurface $Q = 1.3 \times 10^6$ coloured by the x_3-component of the total vorticity.

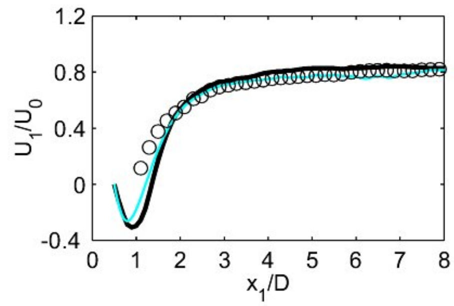

Figure 2. Time-averaged streamwise velocity $\overline{u_1}$ along the line $x_2 = 0$ at $\mathrm{Re}_D = 1.4 \times 10^5$: (———) present simulation , (○ ○ ○) data of Cantwell and Coles,[14] (———) numerical simulation of Breuer[15] (case A3).

B. Acoustic radiation

In order to validate the aeroacoustic calculations and to represent the acoustic waves radiated by the æolian tone, the acoustic fields in a plane (x_1, x_2) corresponding to the surface and the volume terms of equation (2) are plotted in figure 3. The visualisation mesh is based on a circular unstructured grid composed of about 3200 points extending from the boundaries of the aerodynamic domain up to $r_x = 64D$. The structure of the diffracted field (figure 3(a)) is dipolar with a dominent frequency f_0. The feature of the direct field (figure 3(b)) is quadrupolar and controlled also by the frequency f_0. The surface term represents about 80-90% of the total radiation in the direction perpendicular to the flow ($\theta = 90^o$). This result is similar to our previous 2-D result.[1]

In figure 4 are plotted directivity patterns of the overall sound pressure level. The quadrupolar directivity of the volume term is not so marked than in 2-D studies because of the 3-D nature of the flow. All the sources are much less correlated in time and space than for the 2-D case, and the radiated sound is no longer dominated by strong organized diffraction effects.

Acoustic spectra are displayed in figure 5 for three observation angles, $\theta = 0^o$, 45^o and 90^o) respectively. As shown in these figures, and confirming the analysis of the directivity patterns, the æolian tone phenomenon ($f \approx 400$ Hz) is completly controled by the surface term. The conclusions are however quite different for frequencies above 1500 Hz : the surface contribution becomes less efficient than the volume term. For high frequencies, the direct field seems to be the main contributor.

The advanced time algorithm, adapted to low Mach number configuration, reveals on this 3-D test case all its advantages allowing the calculation of the volume integral in very reasonable computational times. Moreover, this application shows that the calculation of the volume integrals would be required to obtain a good estimation of the broadband noise in low Mach number configurations.

IV. Experimental and numerical study of a wall-mounted half cylinder

The following test case is a simplified automotive geometry, *i.e.* a side mirror modeled as a wall-mounted half cylinder. The study is divided into two parts : the first one presents the measurements performed in

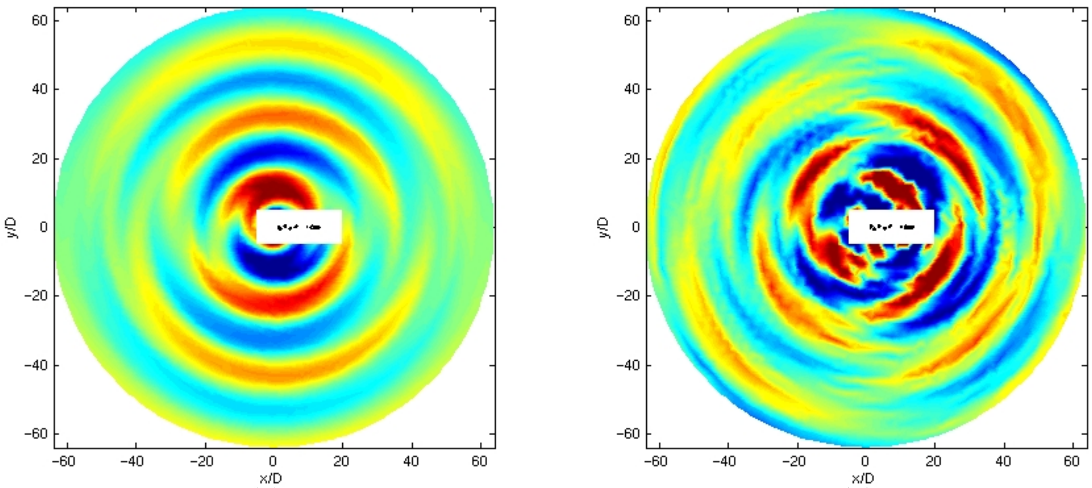

Figure 3. Acoustic pressure predicted by the FW-H's analogy : (a) contribution of the surface integral (levels of pressure between -1.0 Pa and $+1.0$ Pa); (b) contribution of the volume integral (levels of pressure between -0.1 Pa and $+0.1$ Pa).

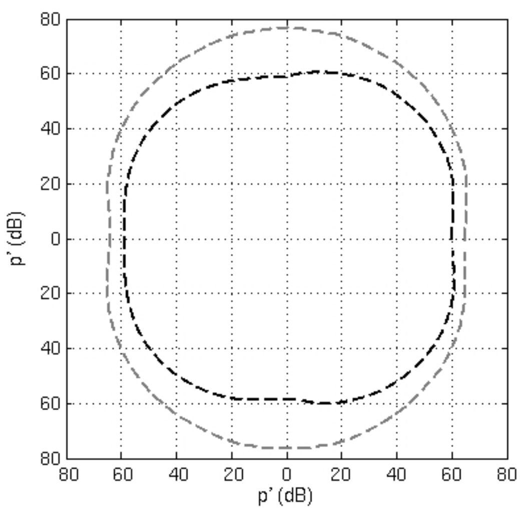

Figure 4. Overall sound pressure level directivity patterns at $r_x = 64D$: (▬ ▬ ▬), volume integral part; (▬ ▬ ▬), surface integral part.

the Ecole Centrale de Lyon's anechoic wind-tunnel involving both the characterisation of the flow and of the noise measurements. The second part is a numerical study in which the aerodynamic simulation is presented and the acoustic calculations are compared to the measurements.

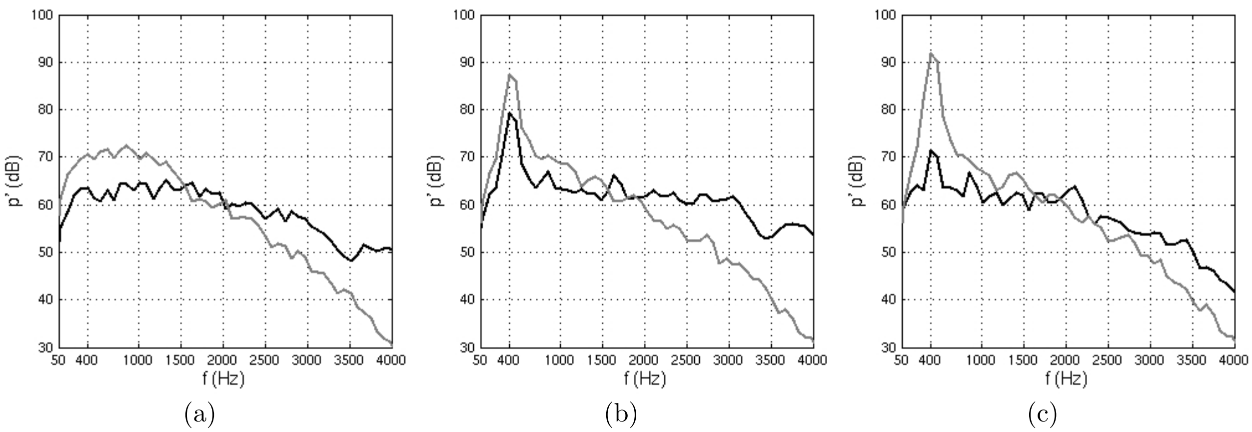

Figure 5. Acoustic pressure spectra of : (———) the volume contribution; (———) the surface contribution at (a) $\theta = 0^o$; (b) $\theta = 45^o$ and (c) $\theta = 90^o$.

A. Experimental study

1. General settings

The diameter of the half cylinder in $D = 10$ cm and its height $H = 2D$, the aspect ratio H/D is about the same as a real side mirror (see figure 6(a)). The mean flow speed is $U_\infty = 40$ m/s in the x_1-direction corresponding to the speed of automotives on highways. The corresponding Reynolds number based on the diameter of the half-cylinder is Re$= 2.7 \times 10^5$ and the Mach number M$= 0.18$. The flow can be considered as incompressible.
The size of the wind-tunnel is 50×50 cm and the lateral walls are drawn in order to follow the streamlines of the mean flow and to limit the blockage effects. The shape of these lateral walls were obtained using a preliminary steady calculation. The lateral and upper walls are acoustically transparents to allow acoustic measurements in the far-field and are visible in figure 6(b).
Hot wire anemometry measurements characterize the incoming flow : the turbulent rate in the middle of the wind-tunnel is less than 1% and the thickness of the turbulent boundary layer is about 5 cm. The symmetry of the boundary layer is verified $8D$ upstream of the half cylinder, and it is about constant for three x_1-positions ($x_1 = -16D, \ -12D$ and $-8D$).

2. Aerodynamic measurements

The aim of the aerodynamic measurements is to qualify both the steady and the unsteady aerodynamic flow. The flow is investigated by using Particle Image Velocimetry (PIV) in (x_1, x_2) and (x_1, x_3) planes corresponding to horizontal and vertical planes. The mean velocities and the fluctuations are then available for about 50 different planes by averaging up to 1000 instantaneous fields. As shown in figure 7, the maximum recirculation length is about $L_f = 1.7D$ for $x_2 = 0.5D$ and the symmetry of the wake is verified.
In the wake of the half-cylinder, hot-wire acquisitions give results in (x_2, x_3) planes and spectra of the u_1-velocity component. These spectra point out the presence of a periodic vortex shedding linked to the cylinder diameter with the frequency $f_0 = 72$ Hz. In the upper shear layer, the frequency of the instability is $f_{SL} = 225$ Hz.
The static pressure is measured on the floor and on the half-cylinder. The pressure coefficient C_p is independent of the inflow speed and no problem of transition is involved in the experiments. A representation of the pressure coefficient C_p is plotted in figure 8, the recirculation length is $1.5D$. The depression just behind

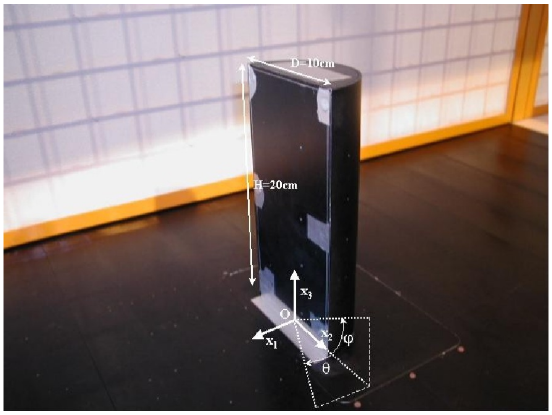

(a)

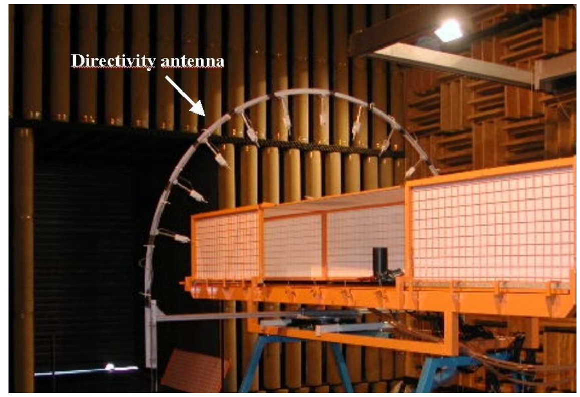

(b)

Figure 6. Pictures of the half-cylinder and of the ECL's wind-tunnel used for the experiments presented here. In figure (b), the azimuth of the directivity antenna is $\theta = +20^o$ and the 11 microphones are equally located from $\varphi = 15^o$ to $\varphi = 175^o$.

the half-cylinder is relatively strong and the minimum pressure coefficient value is $C_{pmin} = -0.61$.
The flow is also characterised in term of pressure fluctuations for 128 positions by using electret microphones up to $f = 4 - 5$ kHz. The whole pressure fluctuation measurements have been performed simultaneously so that coherences between each signals can be measured. Low level of coherence is observed between the signals excepted at the vortex shedding frequency f_0. The low frequency coherence spectra ($f < 500$ Hz) located in the recirculation zone look like those in a turbulent boundary layer.

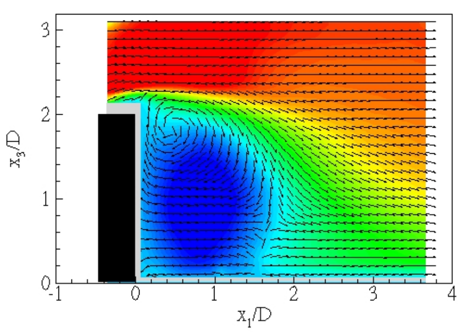

Figure 7. $\bar{u_1}$ velocity field measured by PIV in the plane $x_2 = 0$ (levels between -10 and 40 m/s) and direction of the total velocity in this plane (one vector on two is plotted).

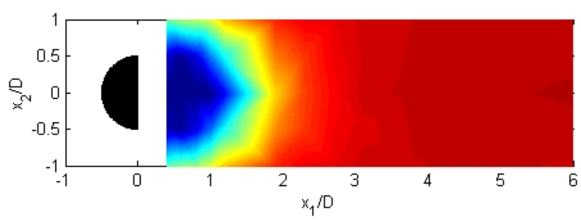

Figure 8. Pressure coefficient C_p in the wake of the half-cylinder (levels between -0.5 and 0.0).

3. *Acoustic Radiation*

As shown in figure 6(b), 11 microphones equally located on a 1 m circular beam rotating around the x_3-axis are used to measure the radiated sound. The position of the microphones is defined by using two angles θ

and φ as shown in figure 6(a). The noise with and without the half-cylinder is measured. The wind-tunnel is shown to be noisy and the noise generated by the half-cylinder is not easy to identify excepted for the frequency f_0 which emerges of 3-5 dB on the acoustic spectra for $-20^o \leq \theta \leq +20^o$ and $15^o \leq \varphi \leq 45^o$ (respectively $145^o \leq \varphi \leq 175^o$). The broadband noise of the cylinder is of the same order of magnitude as the background noise.
Some coherences are measured between the outflow microphones and both the wall pressure sensors and the hot-wire. The only striking result observed is a coherence of about 0.8 at the frequency f_0. This phenomenon carries the same relevance in both aerodynamics and acoustics alike, following the law St$= Df_0/U_\infty$ with St$= 0.20$. Moreover, the related sound level follows a law in about six power of the velocity which is similar to the æolian tone phenomenon. This vortex shedding is hence a good way to validate an unsteady simulation.

The whole aerodynamic and acoustic database provides a lot of information useful for both understanding the flow and validating the aeroacoustic calculation. In the next part, the corresponding aerodynamic simulation is presented and the acoustic calculation is carried out using equation (2).

B. Computation and validation of the flow

1. Properties of the simulation

The flow over the half-cylinder previously presented is simulated by using the LES of Fluent 6.1 with a Smagorinsky constant fixed to $C_s = 0.1$. The aerodynamic domain is represented in figure 9. The lateral and upper limit conditions are periodics, a pressure condition is imposed at the outlet, and the velocity profile measured by hot-wire is imposed as inflow condition. The initial flow is laminar and the velocity fixed to $U_\infty = 40$ m/s in the x_1-direction.
The unstructured meshgrid is composed of about 10^6 nodes and 3.5×10^6 tetrahedrical cells. The characteristic length used to discretise the surface of the half-cylinder is 1.2×10^{-3} m. The temporal algorithm is implicit and based on a centred scheme of second order. The time step of the calculation is $\Delta t = 2.5 \times 10^{-5}$ s and the aerodynamic data (u_i and p) are recorded during 0.3 s every 4 temporal iterations on each point of the mesh-grid.

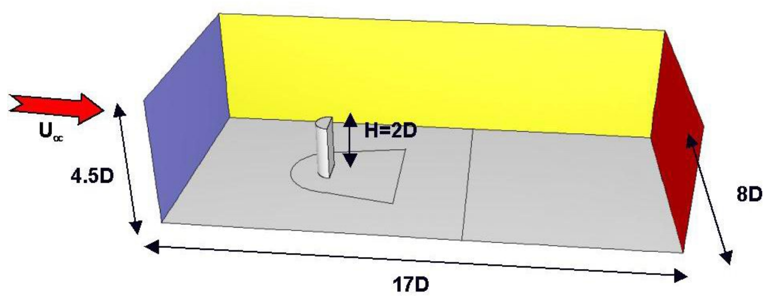

Figure 9. Aerodynamic domain used to perform the LES around the half-cylinder at Re= 2.7×10^5 **and M=** 0.18.

2. Validation of the CFD

The instantaneous flow is represented in figure 10 through a snapshot of the Q-criterion. The structures displayed in this figure are periodically shed from the half-cylinder with the frequency $f_0 = 78$ Hz and correspond to the phenomenon experimentally detected and also numerically observed by Lee *et al.*[18] The analysis of the Q-criterion shows that these structures are generated as the Kármán streets and are deformed by the mean flow about $2D$ downstream in the wake. The difference of 8% in the value of f_0 can be attributed to the inlet velocity profile and more particularly to the thickness of the impinging boundary layer. Indeed, a first simulation was performed with a boundary layer of only 1 cm and the frequency f_0 was about 85 Hz. The upper shear layer structures are also present in the calculation with a frequency $f_{SL} = 240$ Hz.

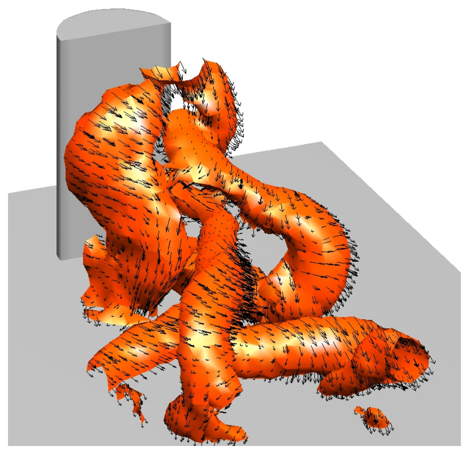

Figure 10. Perspective view of the Q-criterion (isosurface $Q = 5 \times 10^5$ with velocity vectors).

In figure 11(a) the mean velocity $\bar{u_1}/U_\infty$ along the line $x_2 = 0$ and $x_3 = 1D$ are plotted and compared to the PIV measurements. The numerical recirculation length, about $1.9D$ instead of $1.7D$, is slighty overestimated as for the cylinder application but the shapes are very similar. The turbulence intensities are of the same order and, as shown in figure 11(b), the maximum of fluctuations appears just after the recirculation zone. This zone corresponds to the position of the vortex shedding and its intensity is well predicted.

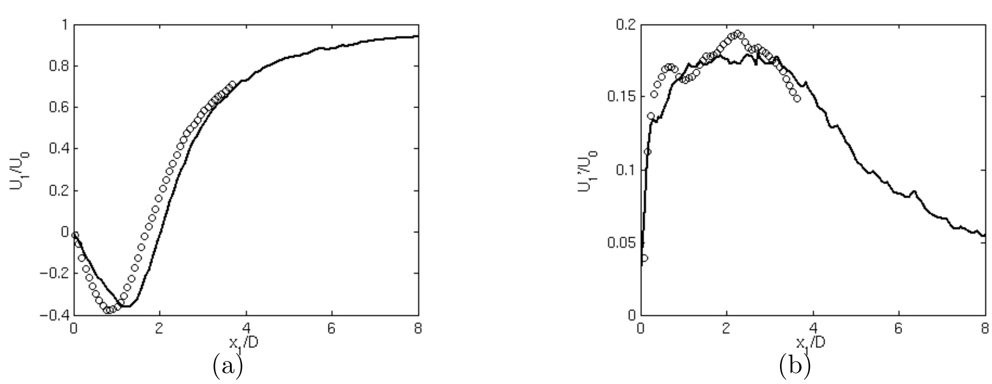

Figure 11. Profiles of mean and fluctuating u_1 velocity component along $x_2 = 0$ and $x_3 = 1D$: (———) present simulation, (○ ○ ○) experimental PIV data

The pressure coefficient is represented in figure 12. The comparison with the experiments is also very satisfactory particularly the lowest value of C_p, $C_{pmin} = -0.62$, yielding an error less than 2%. In figure 13, pressure fluctuation power spectral density are plotted. First, the vortex shedding is well emerging from the numerical spectrum and a difference of about 2 dB is found. Second, the pressure fluctuations are in good agreement up to 1500-2000Hz. For higher frequencies, the discrepancy may correspond both to the limits of the calculation and also to the limits of the measurements.

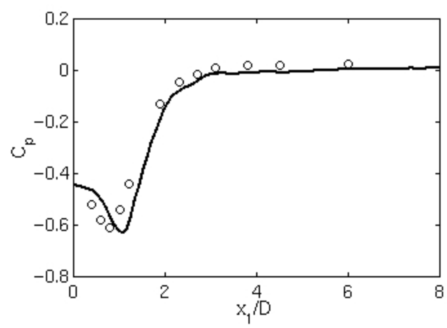

Figure 12. Pressure coefficient on the floor ($x_3 = 0$) along $x_2 = 0$: (——) present simulation, (○ ○ ○) experimental PIV data

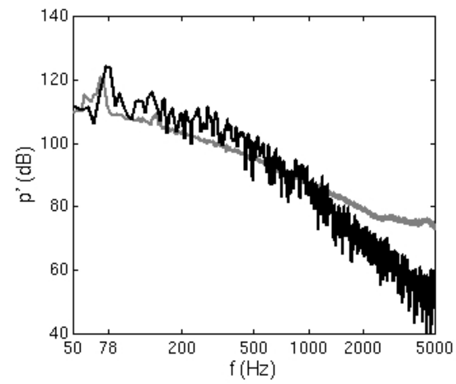

Figure 13. Pressure fluctuation PSD in $x_1/D = 2$ and $x_2/D = 0.5$ where the velocity fluctuations are the strongest : (——) present simulation, (— — —) wall pressure fluctuation measurements.

Aerodynamic results are in good agreement with the measurements up to 1500 Hz and can now be used as an input for the acoustic analogy.

C. Evaluation of the radiated sound

The major difficulty of this aeroacoustic calculation is to correctly take into account the influence of the floor. Indeed, the effect of an infinite plane in presence of a flow is only the reflection of the acoustic waves radiated by the source volume.[9,19,20] Numerically, for low Mach number flows, these reflections are included in the surface integral of equation (2) in two cases : either the CFD is compressible,[8] or a particular diffraction problem as the æolian tone is considered.[1] Since the previous simulation is incompressible, the calculation of the floor integral is hence not correct. The acoustic radiation is then studied as follows. First, the direct radiation is estimated by solving the volume integral of equation (2). Then, the reflections by the floor are considered as the radiation corresponding to the image of the volume source by the plane. Lastly, to point out the influence of the half-cylinder and particularly the diffraction phenomena, the surface integrals over the half-cylinder and its image by the floor are computed.

The sound is estimated by using the previous LES aerodynamic database which corresponds to a physical time of 0.3 s with a sampling rate of 10 kHz. The sound is computed for an observer located at $M_1 = (\theta_1{=}0^o, \varphi_1{=}30^o)$ where the tone is the most emerging. The total acoustic pressure on M_1 is plotted in figure 14. As shown by these PSD spectra, the estimation of the radiated sound is satisfying above 1000 Hz. The discrepancy between numerical and experimental results is about 10 dB up to 1000 Hz and is about 5 dB at the frequency f_0.
In figure 15, the direct, the reflected and the half-cylinder contributions are separated. The contributions of the half-cylinder are negligible for all the frequencies, even at the tone. For low frequencies ($f < 750$ Hz), the reflections are very constructive (+6 dB) and increase significatively the spectrum levels. This would show that the tone is not due to the diffraction of the acoustic waves by the half-cylinder but is due both to the source volume radiation and to its reflection by the floor.
Complementary works have to be performed in order to determine the origin of such low frequency differences. Indeed, on the one hand the wind-tunnel was noisy and the noise generated by the half-cylinder itself is not easily reachable. On the other hand, the proposed analysis of the radiated sound may be improved.

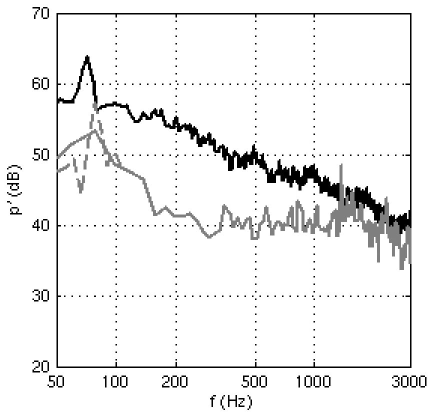

Figure 14. Comparison of the PSD of the radiated sound for an obsverver located at $M_1 = (\theta_1{=}0^o, \phi_1{=}30^o)$: (——) acoustic measurements; (——) estimation of the radiated sound with a broadband spectral analysis (Δf = 20 Hz) and (– – –) estimation of the radiated sound with a low frequency analysis ($\Delta f = 5$ Hz). The pressure of reference $p_0 = 2 \times 10^{-5}$ Pa is used.

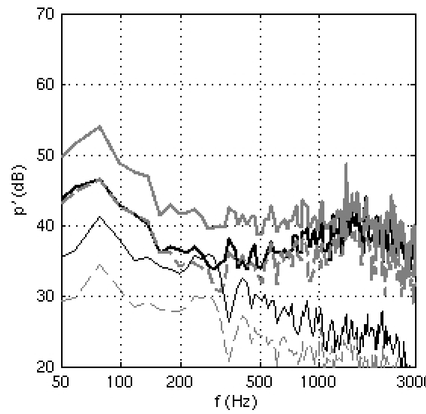

Figure 15. Separation of the contributions constituting the acoustic radiation for M_1 : (——) Contribution of the source volume, (– – –) Contribution of the image of the source volume by the floor, (——) Contribution of the surface integral over the half-cylinder, (– – –) Contribution of the image of the surface integral over the half-cylinder, (——) Total acoustic radiation given by the sum of the 3 previous contributions.

V. Conclusion

In this article, the development of the resolution of the FW-H's equation using an advanced-time approach is validated. This method allows a spatial and temporal study of the radiated sound as well as the contribution of both the direct and the diffracted fields respectively provided by the volume and the surface integrals. Applied in a first step to a 3-D cylinder flow, this approach confirms that the æolian tone is well described by the surface contribution. The origin of the broadband noise above 1000 Hz is less obvious and the calculation of the volume term is required even for low Mach number applications.
In a second step, a wall-mounted half-cylinder representing a simplified automotive case is studied involving both experimental and numerical analyses. The unsteady CFD results are quite satisfactory compared to the measurements. By using these data as an input, the present CAA method is applied and gives an interesting estimation of the radiated sound up to 3 kHz. As for the cylinder case, the direct radiation seems responsible for the high frequency broadband noise. Nevertheless this point requires further investigations.

References

[1] Pérot, F., Gloerfelt, X., Auger, J., Giardi, H., and Bailly, C., "Numerical prediction of the noise radiated by a cylinder," *AIAA Paper 2003-3240*, 2003.

[2] Ffowcs Williams, J. and Hawkings, D., "Sound generated by turbulence and surfaces in arbitrary motion," *Philosophical Transactions of the Royal Society*, Vol. A264, No. 1151, 1969, pp. 321–342.

[3] Di Francescantonio, P., "A new boundary integral formulation for the prediction of sound radiation," *J. Sound Vib.*, Vol. 202, No. 4, 1997, pp. 491–509.

[4] Brentner, K. and Farassat, F., "Modeling aerodynamically generated sound of helicopter rotors," *Progress in aerospace*

sciences, Vol. 39, No. 8, 2003, pp. 83–120.

[5]Bogey, C. and Bailly, C., “A family of low dispersive and low dissipative explicit schemes for flow and noise computations,” *J. Comput. Phys.*, Vol. 194, No. 1, 2003, pp. 194–214.

[6]Wang, M., Lele, S., and Moin, P., “Computation of quadrupole noise using acoustic analogy,” *AIAA Journal*, Vol. 34, No. 11, 1996, pp. 2247–2254.

[7]Bogey, C., Bailly, C., and Juvé, D., “Noise investigation of a high subsonic, moderate Reynolds number jet using a compressible LES,” *Theoret. Comput. Fluid Dynamics*, Vol. 16, No. 4, 2003, pp. 273–297.

[8]Gloerfelt, X., Bailly, C., and Juvé, D., “Direct computation of the noise radiated by a subsonic cavity and application of integral methods,” *J. Sound Vib.*, Vol. 266, 2003, pp. 119–146.

[9]Ffowcs Williams, J. and Hall, L., “Aerodynamic sound generation by turbulent flow in the vicinity of a scattering half-plane,” *J. Fluid Mech.*, Vol. 40, 1970, pp. 657–670.

[10]Crighton, D. and Leppington, F., “On the scattering of aerodynamic noise,” *J. Fluid Mech.*, Vol. 46, No. 3, 1971, pp. 577–597.

[11]Piomelli, U. and Balaras, E., “Wall-Layer Models for Large-Eddy Simulation,” *Ann. Rev. Fluid Mech.*, Vol. 34, 2002, pp. 349–374.

[12]Cabot, W. and Moin, P., “Approximate wall boundary conditions in the Large-Eddy Simulation of high Reynolds number flow,” *Flow, Turbulence and Combustion*, Vol. 63, 2000, pp. 269–291.

[13]Batham, J., “Pressure distributions on circular cylinders at critical Reynolds number,” *J. Fluid Mech.*, Vol. 57, 1973, pp. 209–228.

[14]Cantwell, B. and Coles, D., “An experimental study of entrainment and transport in the turbulent near wake of a circular cylinder,” *J. Fluid Mech.*, Vol. 136, 1983, pp. 321–374.

[15]Breuer, M., “A challenging test case for LES: high Reynolds number circular cylinder flow,” *International Journal of Heat and Fluid Flow*, 2000, pp. 648–654.

[16]Tremblay, F., *Direct and Large-Eddy Simulation of flow around a circular cylinder at subcritical Reynolds number*, Ph.D. thesis, Technical University of Munich, 2001.

[17]Wang, M., Catalano, P., and Iaccarino, G., “Prediction of high Reynolds number flow over a circular cylinder using LES with wall modeling,” *Center for Turbulence Research, Annual Research Briefs*, 2001, pp. 45–50.

[18]Lee, S., Han, J., Choi, J., and Runchai, A., “A large-eddy simulation of the turbulent flow in the vinicity of an upright wall-mounted half cylinder and aerodynamic sound prediction,” *ASME, FEDSM99*, 1999-7800.

[19]Powell, A., “Aerodynamic noise and the plane boundary,” *J. Acoust. Soc. Am.*, Vol. 32, No. 8, 1960, pp. 982–990.

[20]Howe, M., *Acoustics of fluid-structures interactions*, Cambridge University Press, 1998.